

# Graphene Nanoribbon Phototransistor: Proposal and Analysis

Victor Ryzhii<sup>1,4</sup>, Maxim Ryzhii<sup>1,4</sup>, Nadezhda Ryabova<sup>1,4</sup>, Vladimir Mitin<sup>2</sup>, and Taiichi Otsuji<sup>3,4</sup>

<sup>1</sup>Computational Nanoelectronics Laboratory, University of Aizu, Aizu-Wakamatsu, Fukushima 965-8580, Japan

<sup>2</sup>Department of Electrical Engineering, University at Buffalo, Buffalo, NY 14260-1920, U.S.A.

<sup>3</sup>Research Institute for Electrical Communication, Tohoku University, Sendai 980-8577, Japan

<sup>4</sup>Japan Science and Technology Agency, CREST, Tokyo 107-0075, Japan

Received September 30, 2008; accepted November 13, 2008; published online April 20, 2009

We consider a concept of a graphene nanoribbon phototransistor (GNR-PT) based on an array of GNRs operating as a photodetector of far-infrared (FIR) and terahertz (THz) radiation. The photodetector has the structure of a GNR field effect transistor with the back and relatively short top gates. To calculate the GNR-PT characteristics, we develop an analytical model of the device. This model generalizes the model we proposed previously by accounting for the possibility of not only the thermionic regime but also the tunneling regime of the GNR-PT operation. Using the developed model, we derive analytical formulas for the source–drain current as a function of the intensity and frequency of the incident radiation and bias voltages, and estimate the detector responsivity. The obtained formulas can be used for detector optimization by varying the dark current, photoelectric current gain, and voltage control of the spectral properties. The dependences of the absorption edge on GNR width and bias voltages can be utilized for the development of multicolor voltage tunable FIR/THz photodetectors. © 2009 The Japan Society of Applied Physics

DOI: 10.1143/JJAP.48.04C144

## 1. Introduction

Interband and intraband (intersubband) transitions are commonly utilized in photodetectors for far-infrared (FIR) and terahertz (THz) ranges of spectrum based on narrow-gap semiconductors and quantum-well structures, respectively.<sup>1,2)</sup> Quantum-dot and quantum-wire intersubband detectors were proposed<sup>3,4)</sup> and realized by many groups. Graphene, i.e., a monolayer of carbon atoms forming a dense honeycomb two-dimensional crystal structure<sup>5,6)</sup> opens up real prospects in the creation of novel not only electron but also optoelectron devices, in particular, novel photodetectors. One of the most promising metamaterials for FIR and THz detectors is a patterned graphene in the form of an array of graphene nanoribbons (GNRs). The energy gap between the valence and conduction bands of GNRs as well as between the intraband subbands can be engineered by varying the shape of GNRs, particularly, their width. The latter can be defined by lithography.

In this paper, we consider a GNR phototransistor (GNR-PT) operating as an FIR/THz photodetector with optical input from the bottom of the structure through the substrate and layer sandwiching the GNR array, develop its analytical device model, and analyze the GNR-PT characteristics using this model. The photodetector under consideration has been proposed recently by us.<sup>7)</sup> It has a structure of a GNR field-effect transistor (FET) consisting of an array of GNRs with the side source and drain contacts sandwiched between the highly conducting substrate and the top gate electrode as shown schematically shown in Fig. 1. The operation of FETs with a similar structure were explored recently (see, for instance, refs. 8–12). The band diagrams of a GNR-PT at a bias back gate voltage  $V_b > 0$ , a top gate voltage  $V_g < 0$ , and a source–drain voltage  $V_d$  in dark conditions and under irradiation are shown in Fig. 2.

The GNR-PT model and its device characteristics as a photodetector were briefly discussed in our recent letter.<sup>7)</sup> Here, we consider the proposed photodetector on the basis of the device model that generalizes the model we used previously.<sup>7)</sup> The proposed model describes both the thermionic and tunneling modes of the GNR-PT operation. At relatively low top gate voltages, the GNR-PT band

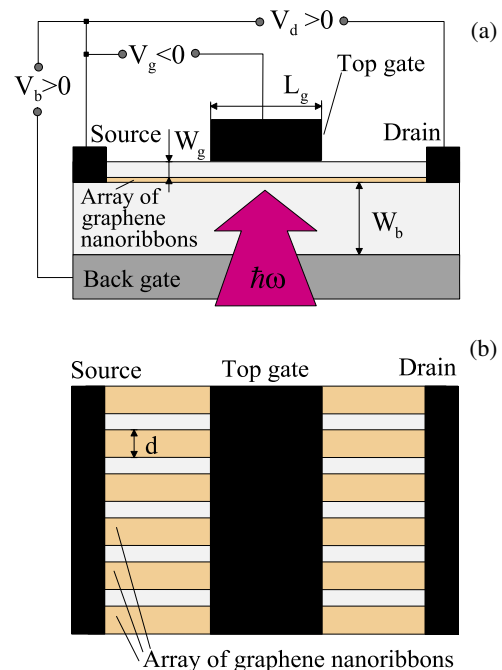
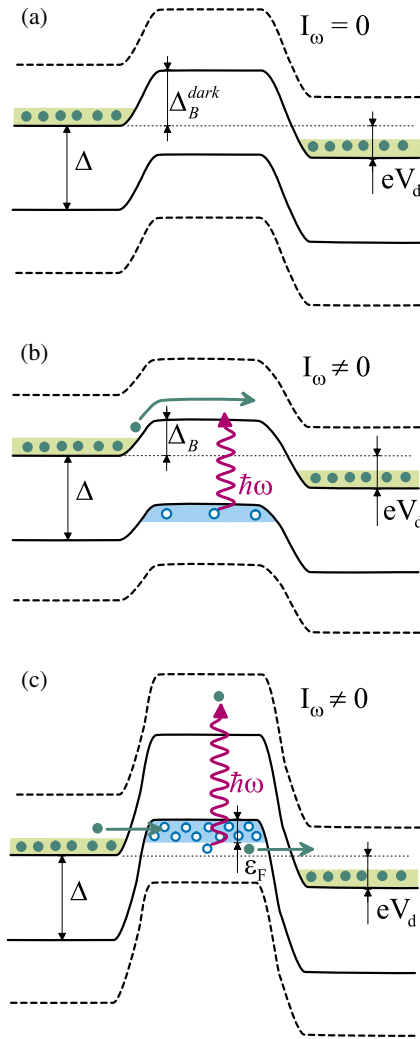


Fig. 1. (Color online) GNR-PT structure side (a) and top (b) schematic views.

structure corresponds to that shown in Figs. 2(a) and 2(b). In this case, the source–drain current is associated with the electrons injected from the source section of the channel and overcoming the potential barrier  $\Delta_B^{\text{dark}}$  (in dark conditions) or  $\Delta_B$  (in the general case, in particular, under irradiation) and, partially, with the electrons injected from the drain section of the channel and overcoming the potential barrier  $\Delta_B^{\text{dark}} + eV_d$  (or  $\Delta_B + eV_d$ ), where  $e$  is the electron charge. The variation in the barrier height from  $\Delta_B^{\text{dark}}$  to  $\Delta_B$  and, hence, the variation in the source–drain current, are associated with the charging of the channel section under the top gate (gated section) by the photogenerated holes. The value of this charge is determined by the density of photogenerated holes, which, in turn, is determined by the balance between the rate of the photogeneration of holes and the rate of their thermionic escape from the gated section to the source and



**Fig. 2.** (Color online) GNR-PT band diagrams at  $V_b > 0$ ,  $V_g < 0$ , and  $V_d > 0$  under dark conditions (a) and under irradiation at relatively low (b) and high (c) top-gate voltages. Fundamental (solid lines) and first (dashed lines) subbands of the GNR conduction and valence band are shown. Opaque and open circles correspond to electrons and holes, respectively.

drain sections. This mechanism is referred to as the thermionic mechanism. If the bias of the top gate is sufficiently strong, the n-p and p-n junctions near the source and drain edges of the gated regions are formed as shown in Fig. 2(c). In such a case, the source-drain current might be determined by interband tunneling through these n-p and p-n junctions. In this situation, when  $\Delta_B^{\text{dark}}$  and  $\Delta_B$  are relatively large, the thermionic current can be disregarded.

GNRs exhibit the energy spectra of electrons and holes consisting of a series of the subbands with a gap  $\Delta$ , which essentially determines the photodetector spectral properties. The latter depends on the GNR width  $d$ . For simplicity, we assume  $\epsilon_n^\pm(p) = \pm v \sqrt{p^2 + (\pi\hbar/d)^2 n^2}$ . Here,  $v \simeq 10^8$  cm/s is the characteristic velocity of the electron (upper sign) and hole (lower sign) spectra,  $p$  is the momentum along the nanoribbon,  $\hbar$  is the reduced Planck constant, and  $n = 1, 2, 3, \dots$  is the subband index. This spectrum corresponds to the band gap  $\Delta = 2\pi\hbar/d$  between the valence and conduction bands and to a specific density of states in the conduction and valence bands as a function of energy.

## 2. Thermionic Mechanism

When the device band diagram is that shown in Figs. 2(a) and 2(b), the source-drain current along the GNRs is associated with the electrons propagating from the source to the drain and overcoming the barrier in the gated section of the channel. In this case, the source-drain dc current can be calculated using

$$J = \frac{2e}{\pi\hbar d} \int_0^\infty dp v_p [f(p, x) - f(-p, x)], \quad (1)$$

where  $\hbar$  is the reduced Planck constant ( $\hbar = h/2\pi$ ), and  $f(p, x)$  is the electron distribution function. The latter is governed by the Boltzmann equation. Here,  $v_p = p/m^* \sqrt{1 + (2p^2/\Delta m^*)} \simeq p/m^*$  is the electron velocity with a momentum  $p$ ,  $m^* = \Delta/2v$ , and  $v_p$  is the collision frequency of electrons associated with the disorder (including edge roughnesses) and acoustic phonons. We disregard the inelasticity of the scattering on acoustic phonons, so that all the scattering mechanisms under consideration result in the change in the electron momentum from  $p$  to  $-p$ . The probability of electron elastic scattering is essentially determined by the density of state. Taking into account collisional broadening<sup>13,14</sup> (see also refs. 15 and 16), we approximate the dependence in question as  $v_p = v\sqrt{\gamma^2 + 1}/\sqrt{\gamma^2 + (p/p_T)^2}$ , where  $v$  is the collision frequency of thermal electrons,  $\gamma$  characterizes the collisional broadening, and  $p_T = \sqrt{2k_B T m^*}$ . If  $|p|/p_T < \gamma$ ,  $v_p \simeq v\sqrt{\gamma^2 + 1}/\gamma = \text{const}$ , whereas if  $|p|/p_T \gg 1$  (but  $|p| < p_\Delta = \sqrt{2\Delta m^*}$ ), one obtains  $v_p \simeq v\sqrt{\gamma^2 + 1}(p_T/|p|)$ . Solving eq. (1) accounting for the pertinent boundary conditions (assuming for simplicity that  $V_d \ll V_b$ ), one can arrive at the following formula for the source-drain thermionic current:

$$J = J_m G_0 \exp\left(-\frac{\Delta_B}{k_B T}\right) \left[1 - \exp\left(-\frac{eV_d}{k_B T}\right)\right], \quad (2)$$

where  $T$  is the temperature and  $k_B$  is the Boltzmann constant. The characteristic current density  $J_m$  is determined by the electron densities in the source and drain sections. These densities are given, respectively, by  $\Sigma_b = \kappa V_b/4\pi eW_b$  and  $\Sigma_b = \kappa(V_b - V_b)/4\pi eW_b \simeq \kappa V_b/4\pi eW_b$ , where  $\kappa$  is the dielectric constant and  $W_b$  is the thickness of the layer between the back gate and the GNR array [see Fig. 1(a)]. When the electron system in the source and drain sections is nondegenerate,  $J_m = e\Sigma_b v_T$ , where  $v_T \propto v_W \sqrt{k_B T/\Delta} \propto \sqrt{k_B T/m^*}$  is the thermal electron velocity and  $v_W$  is the characteristic velocity of electrons and holes in graphene ( $v_W \simeq 10^8$  cm/s). At high back-gate voltages, the electron system in question can be degenerate, so that  $J_m \propto \exp(\epsilon_F^b/k_B T)$ , where  $\epsilon_F^b \propto (\hbar d v_W \kappa V_b/eW_b)^2/\Delta$  is the electron Fermi energy in the source and drain sections of the channel. The collision factor  $G_0$  is associated with the scattering of electrons propagating along the gated section. The scattering results in the reflection of a portion of the electron flux injected into the gate section, so that generally  $G_0 \lesssim 1$ . In the framework of the model under consideration, one obtains

$$G_0 = \int_0^\infty \frac{d\xi e^{-\sqrt{\xi(\gamma^2 + 1)}}}{\sqrt{\xi(\gamma^2 + 1)} + \beta\sqrt{\gamma^2 + 1}}, \quad (3)$$

where the ballistic parameter  $\beta = vL_g/v_T = \nu\tau$ , where  $L_g$  is

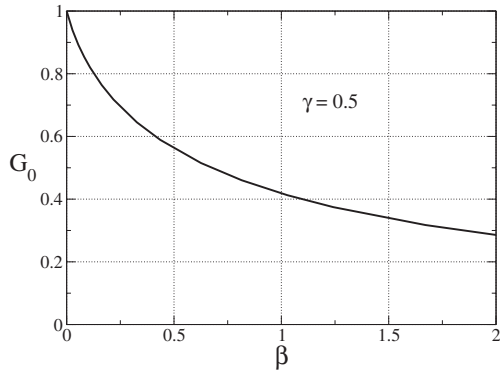


**Fig. 3.** Collision factor  $G_0$  vs ballistic parameter  $\beta = \nu\tau$ .

the length of the top gate [see Fig. 1(a)] and  $\tau$  is the electron transit time. Figure 3 shows the  $G_0$  vs  $\beta$  dependence calculated using eq. (3) for  $\gamma = 0.5$ .

The equation governing the balance of the holes photo-generated by absorbed radiation can be presented as

$$\Sigma_g \exp\left(-\frac{\Delta_B}{k_B T}\right) \left[1 + \exp\left(-\frac{eV_d}{k_B T}\right)\right] = \frac{\alpha_\omega I_\omega}{\hbar\omega} \tau. \quad (4)$$

Here (see ref. 7 and the references therein),

$$\alpha_\omega = \alpha \sum_{n=1}^{\infty} \frac{\Delta \cdot \Theta(\hbar\omega - n\Delta)}{\sqrt{\hbar^2\omega^2 - n^2\Delta^2}} \quad (5)$$

is the GNR interband absorption coefficient of the photons with an energy  $\hbar\omega$ ,  $I_\omega$  is the intensity of radiation, and  $\alpha = 2\pi e^2/c\hbar \approx 2\pi/137$ , where  $c$  is the speed of light, and  $\Theta(\hbar\omega)$  is the unity step function.

Considering the relationship between the hole density in the gated region  $\Sigma_g$  and the barrier heights  $\Delta_B^{\text{dark}}$  and  $\Delta_B$  and using eq. (2), we arrive at the following equation for the detector responsivity  $R = \Delta J/L_g I_\omega$ , where  $\Delta J = J - J^{\text{dark}}$ , in the particular case of nondegenerate electron systems in the source and drain sections:

$$R \simeq \alpha G_0 \left(\frac{W}{W_b}\right) \left(\frac{e^2 V_b}{k_B T}\right) \left[\frac{1 - \exp(-eV_d/k_B T)}{1 + \exp(-eV_d/k_B T)}\right] \times \sum_{n=1}^{\infty} \left(\frac{\Delta}{\hbar\omega}\right) \frac{\Theta(\hbar\omega - n\Delta)}{\sqrt{\hbar^2\omega^2 - n^2\Delta^2}}. \quad (6)$$

Here,  $W = W_b W_g / (W_b + W_g)$  with  $W_g$  being the thickness of the layer between the top gate and the GNR array [see Fig. 1(a)]. The divergence on the right-hand side of eq. (6) when  $\hbar\omega$  tends to  $\Delta$  is eliminated owing to the ‘‘smearing’’ of the valence and conduction band edges (by  $\Gamma \sim \hbar\nu$ ) due to disorder. In the most interesting situation when  $\hbar\omega \gtrsim \Delta$  and  $eV_d \gg k_B T$ , eq. (6) yields

$$R \simeq \alpha G_0 \left(\frac{W}{W_b}\right) \left(\frac{e^2 V_b V_d}{k_B^2 T^2}\right) \frac{e}{\sqrt{\hbar^2\omega^2 - \Delta^2}}. \quad (7)$$

It is instructive that the GNR-PT responsivity is independent of  $\Delta_B^{\text{dark}}$  (although the dark current is primarily determined by this quantity). This is because the effective life time of the photogenerated holes in the depleted section of the channel and, therefore, their density increases as  $\exp(\Delta_B^{\text{dark}}/k_B T)$  [see eq. (4)]. An example of the GNR-PT responsivity as a function of the photon energy calculated using eq. (6) is shown in Fig. 4. Assuming  $W \simeq W_b/2$ ,

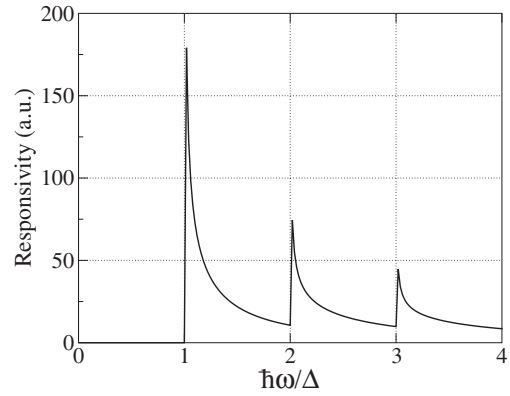


**Fig. 4.** GNR-PT responsivity  $R$  as a function of normalized photon energy  $\hbar\omega/\Delta$ .

$eV_d \gg k_B T$ ,  $G_0 = 0.2$ ,  $\Delta = 50$  meV,  $\Gamma = 2-4$  meV,  $V_b = 1$  V, and  $T = 300$  K, we obtain  $\max R \sim 10-20$  A/W. These responsivities obtained significantly exceed those of inter-subband quantum-well, -wire, and -dot photodetectors in the IR and THz ranges (see, for instance, ref. 2). This is primarily due to a higher quantum efficiency and a higher photoelectric gain, which might be exhibited by GNR-PTs. The latter is associated with a long life time of the photogenerated holes in the central section of the channel because these holes are confined in this section by relatively high barriers, so that the photoelectric gain  $g \gg 1$ . The maximum responsivity of GNR-PTs can also exceed the responsivity of conventional photodetectors made of narrow gap semiconductors (for example, PbSnTe and CdHgTe), whose responsivity is about a few A/W,<sup>1,2)</sup> because the former can exhibit a rather high quantum efficiency at resonances  $\hbar\omega = n\Delta$  arising owing to the lateral quantization in GNRs.

### 3. Tunneling Mechanism

At a high top gate voltage bias when the band diagram corresponds to Fig. 2(c), the source–drain current as well as the leakage current of the photogenerated holes (from the gated section to the the source and drain sections) can be of tunneling origin. In such a situation, the conductance of the gated sections populated by holes (this section is of p-type) is comparable with the conductances of the n-type source and drain sections, i.e., it is fairly high. Hence, the source–drain and leakage currents are determined by the tunneling conductances of the n–p and p–n junctions, so that the potential drops mainly across these junctions. The interband tunneling of electrons and holes through the n–p and p–n junctions results in fact in their recombination.

In the case of the tunneling mechanism, eq. (2) should be replaced by (see, for instance, refs. 17 and 18)

$$J = \sigma_m \exp\left(-\frac{\pi\Delta^2}{\hbar v_{we} E_B}\right) \frac{V_d}{2}, \quad (8)$$

where  $\sigma_m \sim 4e^2/hd$  is the characteristic tunneling conductance and  $E_B$  is the electric field in the n–p and p–n junctions. For a rough estimate one can use set  $E_B \simeq \Delta_B/el_B$ , where  $l_B = W\eta$  is the length of the depleted region in the n–p and p–n junctions. In a situation related to that under consideration  $\eta > 1$  and  $l_B < W$ . Since the formula for  $\eta$ , which

can be obtained from our previous results<sup>7,19</sup> is rather cumbersome, it has been omitted here. Hence, for the barrier electric field variation  $E_B - E_B^{\text{dark}}$ , one obtains

$$E_B - E_B^{\text{dark}} = \frac{\Delta_B - \Delta_B^{\text{dark}}}{e l_B}. \quad (9)$$

Considering eqs. (8) and (9), we obtain

$$\begin{aligned} \Delta J &= \sigma_m \left[ \exp\left(-\frac{\pi \Delta^2}{\hbar v_W e E_B}\right) - \exp\left(-\frac{\pi \Delta^2}{\hbar v_W e E_B^{\text{dark}}}\right) \right] \frac{e V_d}{2} \\ &\simeq \sigma_m \exp\left(-\frac{\pi \Delta^2}{\hbar v_W e E_B^{\text{dark}}}\right) \left(\frac{\pi \Delta^2}{\hbar v_W e E_B^{\text{dark}}}\right) \\ &\quad \times \left(\frac{E_B - E_B^{\text{dark}}}{E_B^{\text{dark}}}\right) \frac{V_d}{2} \\ &\simeq \sigma_m \exp\left(-\frac{\pi \Delta^2}{\hbar v_W e E_B^{\text{dark}}}\right) \left(\frac{\pi \Delta^2}{\hbar v_W e E_B^{\text{dark}}}\right) \\ &\quad \times \left(\frac{\Delta_B - \Delta_B^{\text{dark}}}{\Delta_B^{\text{dark}}}\right) \frac{V_d}{2}. \end{aligned} \quad (10)$$

The balance of holes is governed by (neglecting the quantum capacitance of the hole system in the gated section in comparison with the geometrical capacitance)

$$2\sigma_m \exp\left(-\frac{\pi \Delta^2}{\hbar v_W e E_B^{\text{dark}}}\right) \frac{(\Delta_B^{\text{dark}} - \Delta_B)}{e} = \frac{e L_g \alpha_\omega I_\omega}{\hbar \omega}. \quad (11)$$

After that, using eqs. (10) and (11), we obtain

$$\Delta J \simeq -\left(\frac{\pi e^2 l_B V_d}{4 \hbar v_W}\right) \left(\frac{\Delta}{\Delta_B^{\text{dark}}}\right)^2 \frac{L_g \alpha_\omega I_\omega}{\hbar \omega} < 0. \quad (12)$$

As follows from eq. (12), the irradiation of the GNR-PT operating in the tunneling regime results in a decrease in the source–drain current, i.e., in negative photoconductivity. This effect is associated with a decrease in the barrier electric field  $E_B$  and, hence, in a decrease in the tunneling current when the potential barrier lowers owing to the positive charge of the photoholes accumulated in the gated region.

Taking into account that the hole system in the gated region is degenerate, the interband absorption is affected by the Burstein–Moss shift of the absorption edge.<sup>20</sup> As a result, eq. (5) for the interband absorption coefficient in the spectral range  $\hbar \omega < 2\Delta$  should be replaced by

$$\alpha_\omega = \alpha \frac{\Delta \cdot \Theta(\hbar \omega - \Delta - 2\varepsilon_F)}{\sqrt{\hbar^2 \omega^2 - \Delta^2}}, \quad (13)$$

where  $\varepsilon_F$  is the Fermi energy of holes in the gated section [see Fig. 2(c)]. This Fermi energy markedly increases with increasing top gate bias voltage. Using eqs. (12) and (13), for the detector responsivity somewhat above the threshold of the intersubband absorption in the gated region ( $\hbar \omega \gtrsim \Delta + 2\varepsilon_F$ ), we obtain

$$\begin{aligned} |R| &\simeq \alpha \left(\frac{\pi e l_B V_d}{4 \hbar v_W}\right) \left(\frac{\Delta}{\Delta_B^{\text{dark}}}\right)^2 \frac{e \Delta}{\hbar \omega \sqrt{\hbar^2 \omega^2 - \Delta^2}} \\ &\simeq \alpha \left(\frac{\pi e l_B V_d}{8 \hbar v_W}\right) \left(\frac{\Delta}{\Delta_B^{\text{dark}}}\right)^2 \frac{e}{\sqrt{\Delta \varepsilon_F}}. \end{aligned} \quad (14)$$

As seen from eq. (14), the GNR-PT tunneling responsivity can be rather large owing to a large factor  $g = (\pi e l_B V_d / 4 \hbar v_W)$ , whereas in the tunneling regime, the factor

$(\Delta / \Delta_B^{\text{dark}} \lesssim 1)$ . Indeed, at  $l_B = 100$  nm and  $V_d = 0.1$  V, one obtains  $g \simeq 12.5$ . Taking this into account and assuming that  $\Delta = 50$  meV,  $\Delta_B^{\text{dark}} = 100$  meV, and  $\varepsilon_F = 10$  meV, from eq. (14), we obtain  $|R| \simeq 6.4$  A/W.

#### 4. Discussion

The predominant mechanism of the GNR-PT operation (thermionic or tunneling) depends on the relative value of the following exponential quantities:  $\exp(-\Delta_B / k_B T)$  and  $\exp(-\pi \Delta^2 / \hbar v_W e E_B) \simeq \exp(-\pi l_B \Delta^2 / \hbar v_W \Delta_B)$ . Comparing these quantities and taking into account that the thermionic regime occurs when  $\Delta_B < \Delta$ , one can come to a conclusion that the thermionic mechanism predominates when

$$\frac{T}{T_t} \gg \left(\frac{\Delta_B^{\text{dark}}}{\Delta}\right)^2, \quad (15)$$

i.e., in particular,  $T \sim T_t$ . Here  $T_t = \hbar v_W / \pi k_B l_B$ . Assuming that  $l_B = 100$ – $500$  nm, we obtain  $T_t \simeq 46$ – $230$  K. However, if  $\Delta_B^{\text{dark}} > \Delta$ , the tunneling mechanism might be predominant in a wide range of temperatures.

The GNR-PT responsivity in the thermionic regime can markedly drop with increasing top gate length due to electron scattering [see eqs. (3), (7), and (8) as well as Fig. 2]. As follows from eq. (3), at  $\beta = \nu \tau \gg 1$ ,  $G_0 \propto \beta^{-1} \propto L_g^{-1}$ , so that  $R \propto L_g^{-1}$ . However, the GNR-PT responsivity in the tunneling regime is virtually independent of the top gate length, at least until the conductance of the degenerate hole system in the gated section exceeds the tunneling conductance of the n–p and p–n junctions electrically induced by the top-gate voltage. The latter is true in the case of the ballistic transport of holes in the gated section. In the case when the hole scattering in this section is essential, the above assumption implies that the GNR-PT responsivity is a weak function of the top-gate length when

$$\sigma_m \exp\left(-\frac{\pi \Delta^2}{\hbar v_W e E_B^{\text{dark}}}\right) \ll \frac{e \mu \Sigma_g}{L_g}, \quad (16)$$

where  $\mu$  is the mobility of holes [the term on the right-hand side of eq. (16) is the conductance of the degenerate hole system in the gated section]. This condition is well satisfied when the gate length  $L_g$  is not too large:

$$L_g \ll l_B \left(\frac{\pi^2 \mu \Sigma_g \hbar}{e}\right) \left(\frac{\hbar v_W}{\Delta l_B}\right) \exp\left[\frac{\Delta}{\Delta_B^{\text{dark}}}\right] \left(\frac{\Delta l_B}{\hbar v_W}\right). \quad (17)$$

At  $\Delta = 50$  meV,  $\Delta_B^{\text{dark}} = 100$  meV,  $\mu = (1-2) \times 10^4$  cm<sup>2</sup> V<sup>-1</sup> s<sup>-1</sup>,  $\Sigma_g = 10^{12}$  cm<sup>-2</sup>, and  $l_B = 100$  nm, the latter inequality yields to  $L_g \ll 40$ – $80$   $\mu$ m. An essential contribution of the n–p and p–n junctions to the net resistance of a graphene transistor structure (even without the gap) is observed experimentally (see, for instance, ref. 21). One needs to stress that the GNR-PT characteristics in the tunneling regime substantially depend on the geometry of the device in its central part, particularly, on the length of these junctions  $l_B \propto W$ . Since  $l_B$  and, hence,  $W$  should not be too small, the barriers separating the GNR array and the back and top gates should be sufficiently thick. This implies that the tunneling leakage current from the GNR array to the gates can be effectively suppressed.

Due to the Burstein–Moss shift of the absorption edge in the tunneling regime, there is a possibility of voltage tuning of the GNR-PT spectral characteristics. Indeed, according to

eqs. (15) and (16), the photon energy corresponding to the interband transitions between the top subband in the valence band and the lowest subband in the conduction band is given by  $\hbar\omega = \Delta + 2\varepsilon_F$ . Considering a one-dimensional spectrum of the holes, their Fermi energy in the gated section at sufficiently high top-gate voltages ( $|V_g| \gg V_b W_g / W_b$ ) can be calculated as  $\varepsilon_F \propto (V_b / W_b + V_g / W_g)^2 \propto V_g^2$ .

## 5. Conclusions

In conclusion, we developed a model for the GNR-PTs and calculated their device characteristics. It was shown that GNR-PTs can surpass IR and THz detectors utilizing other types of quantum structures (particularly, intersubband quantum-well, -wire, and -dot photodetectors). The GNR-PTs under consideration can exhibit substantial technological advantages, including easier integration with readout circuits, over detectors based on narrow-gap semiconductors like PbSnTe and CdHgTe.

## Acknowledgments

The work was supported by the Japan Science and Technology Agency, CREST, Japan. The work at University at Buffalo was partially supported by the Air Force Office of Scientific Research, U.S.A.

- 1) A. Rogalski: *Infrared Phys. Technol.* **38** (1997) 295.
- 2) *Intersubband Infrared Photodetectors*, ed. V. Ryzhii (World Scientific, Singapore, 2003).
- 3) V. Ryzhii: *Semicond. Sci. Technol.* **11** (1996) 759.
- 4) V. Ryzhii, I. Khmyrova, M. Ryzhii, and M. Ershov: *J. Phys. IV* **6** (1996) C3-157.
- 5) C. Berger, Z. Song, T. Li, X. Li, A. Y. Ogbazhi, R. Feng, Z. Dai, A. N. Marchenkov, E. H. Conrad, P. N. First, and W. A. de Heer: *J. Phys. Chem.* **108** (2004) 19912.
- 6) K. S. Novoselov, A. K. Geim, S. V. Morozov, D. Jiang, M. I. Katsnelson, I. V. Grigorieva, S. V. Dubonos, and A. A. Firsov: *Nature* **438** (2005) 197.
- 7) V. Ryzhii, V. Mitin, M. Ryzhii, N. Ryabova, and T. Otsuji: *Appl. Phys. Express* **1** (2008) 063002.
- 8) B. Obradovic, R. Kotlyar, F. Heinz, P. Matagne, T. Rakshit, M. D. Giles, M. A. Stettler, and D. E. Nikonov: *Appl. Phys. Lett.* **88** (2006) 142102.
- 9) Z. Chen, Y.-M. Lin, M. J. Rooks, and P. Avouris: *Physica E* **40** (2007) 228.
- 10) G. Fiori and G. Iannaccone: *IEEE Electron Device Lett.* **28** (2007) 760.
- 11) V. Ryzhii, M. Ryzhii, and T. Otsuji: *Appl. Phys. Express* **1** (2008) 013001.
- 12) V. Ryzhii, M. Ryzhii, A. Satou, and T. Otsuji: *J. Appl. Phys.* **103** (2008) 094510.
- 13) S. Briggs and J. P. Leburton: *Phys. Rev. B* **38** (1988) 8163.
- 14) S. Briggs, B. A. Mason, and J. P. Leburton: *Phys. Rev. B* **40** (1989) 12001.
- 15) G. Pennington and N. Goldsman: *Phys. Rev. B* **68** (2003) 045426.
- 16) J. Guo and M. Lundstrom: *Appl. Phys. Lett.* **86** (2005) 133103.
- 17) A. Ossipov, M. Titov, and C. W. J. Beenakker: *Phys. Rev. B* **75** (2007) 241401.
- 18) L. M. Zhang and M. M. Fogler: *Phys. Rev. Lett.* **100** (2008) 116804.
- 19) V. Ryzhii, M. Ryzhii, and T. Otsuji: *Phys. Status Solidi A* **205** (2008) 1527.
- 20) J. I. Pankove: *Optical Processes in Semiconductors* (Dover Publications, New York, 1971).
- 21) B. Huard, J. A. Sulpizio, N. Stander, K. Todd, B. Yang, and D. Goldhaber-Gordon: *Phys. Rev. Lett.* **98** (2007) 236803.